Sorting out Semiconducting Single-Walled Carbon Nanotube Arrays by Preferential Destruction of Metallic Tubes Using Xenon-Lamp Irradiation

Yongyi Zhang, Yi Zhang, Xiaojun Xian, Jin Zhang,* and Zhongfan Liu*

Center for Nanoscale Science and Technology (CNST), Beijing National Laboratory for Molecular Sciences (BNLMS), Key Laboratory for the Physics and Chemistry of Nanodevices, State Key Laboratory for Structural Chemistry of Unstable and Stable Species, College of Chemistry and Molecular Engineering, Peking University, Beijing 100871, People's Republic of China

Received: November 8, 2007; In Final Form: December 24, 2007

We report herein a simple and reliable approach to prepare densely packed, well-aligned individual semiconducting single-walled carbon nanotube (s-SWNT) arrays using long-arc xenon-lamp (Xe-lamp) irradiation. The densely packed, well-aligned individual SWNT arrays (the mean density was ∼20 tubes/μm) were first grown on a-plane sapphire using ethanol containing 3 wt % water as the carbon source. It is found that water plays a key role in the improvement of the density and the alignment of the SWNT arrays. The densely packed aligned SWNT arrays were then irradiated by a long-arc Xe lamp. Atomic force microscopy manipulation, Raman spectroscopy, and electrical transport measurement revealed that the SWNTs with small diameters ($d < 1$ nm) and the metallic SWNTs (m-SWNTs) in the arrays can be preferentially destroyed, thus leaving s-SWNT arrays on the surface. In general, for the SWNTs with diameters in the region of 1.15−1.55 nm, the percentage of s-SWNTs increased from ca. 50% to 95% after 60 min of irradiation. In situ $I-V$ measurement indicated that, with longer irradiation time, the on/off ratios of the field effect transistors fabricated by the as-grown SWNT arrays increased from below 10 to well above 2000. This change clearly indicated that the m-SWNTs were destroyed faster than the s-SWNTs.

Downloaded via PEKING UNIV on June 30, 2020 at 05:29:54 (UTC).
See https://pubs.acs.org/sharingguidelines for options on how to legitimately share published articles.

Introduction

Single-walled carbon nanotubes (SWNTs) have been regarded as the best candidates for applications in nanoelectronic devices due to their high mobilities (normally more than 10 times larger than that of silicon), high current-carrying capacities (∼10^9 A cm^{-2}), and superb subthreshold characteristics in single-tube transistors.[1−4] Although these properties can be significant for many applications in electronics, optics, sensing, and other fields,[5−11] there still remain a lot of challenges because many applications have a low tolerance for the variations in carbon nanotube diameter or electrical properties that are unavoidable with the current manufacturing methods.

Generally, only semiconducting SWNTs (s-SWNTs) are desired for the fabrication of high-performance field effect transistors (FETs) since metallic SWNTs (m-SWNTs) will lead to electrical shorts in these devices. Unfortunately, SWNTs produced by the methods of chemical vapor deposition (CVD), laser ablation, and arc discharge are mixtures of m- and s-SWNTs, normally containing about 1/3 m-SWNTs. Even if the selective synthesis of m-SWNTs or s-SWNTs is still in its infancy, many efforts have been made to push forward. Several approaches have been developed to obtain s-SWNTs, including solution-phase separation, electrical breakdown of m-SWNTs, and selective growth of certain types of nanotubes.

For the solution-phase separation, various approaches have been used to sort out s-SWNTs, including the selective separation of DNA-wrapped[12−14] or cosurfactant-encapsulated carbon nanotubes (CNTs)[15] and the selective reaction/modification with CNTs.[16−18] However, all of these separation methods involve complicated physical and/or chemical processes, which inevitably bring contamination and degradation to the carbon nanotubes. In the case of electrical breakdown, m-SWNTs in FETs can be burned off due to the Joule heat generated by the current passing through the metallic tubes while the s-SWNTs are turned off by a positive gate voltage.[19] Unfortunately, this approach is ineffective and if the s-SWNTs are in contact with the m-SWNTs, they will be destroyed as well. As for the selective growth,[20,21] s-SWNTs can be produced with a percentage of nearly 90% by plasma-enhanced CVD, but the efficiency still needs to be improved.

Recently, Dai's group[22] reported a gas-phase plasma hydrocarbonation reaction to selectively etch metallic nanotubes, retaining semiconducting nanotubes in a near-pristine form. Within this process, nearly 100% semiconducting nanotubes were obtained when pristine SWNTs with diameters smaller than 1.8 nm were used. Another approach was reported by Huang et al.;[23] that is, using laser irradiation in air, m-SWNTs with certain diameters in a carbon nanotube thin film can be destroyed with an appropriate laser wavelength and intensity. From the above investigations, it seems that the selective harvesting of s-SWNTs can indeed occur. However, little is known so far about the mechanism behind the selection.

To fabricate high-current and high-speed nanotube FETs, densely aligned s-SWNT arrays on the surface are highly desirable.[7,24] Horizontally aligned SWNT arrays on the surface have been achieved with the assistance of gas flow,[25,26] an external electric field,[27,28] special substrates such as sapphire and quartz,[29−35] or postgrowth approaches, such as orientationally selective laser ablation[36] and assembly of SWNT arrays from the solution phase.[37−40]

* To whom correspondence should be addressed. (J.Z.) Phone and fax: 86-10-6275-7157. E-mail: jinzhang@pku.edu.cn.

10.1021/jp710691j CCC: $40.75 © 2008 American Chemical Society
Published on Web 02/20/2008

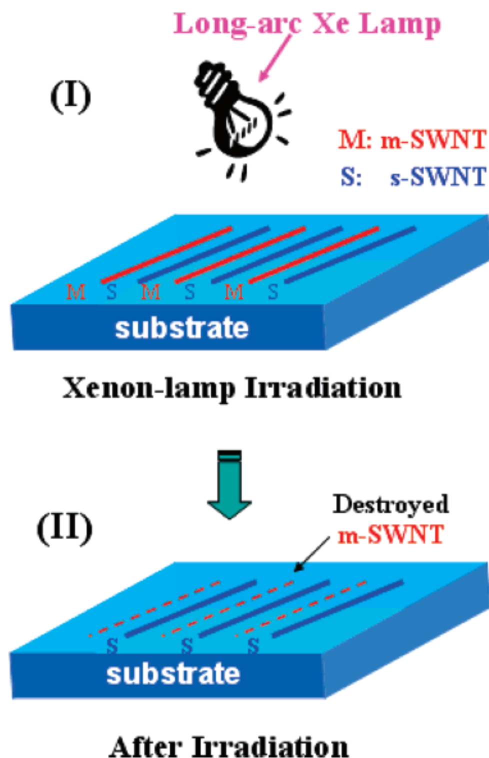

Figure 1. Schematic illustration of the idea of sorting out s-SWNT arrays using long-arc Xe-lamp irradiation. (I) The SWNT arrays are exposed to a long-arc Xe lamp for a certain period of time. The power intensity is ~75 mW/cm^2 on the SWNT arrays. (II) The m-SWNTs (red, M) in the arrays are preferentially destroyed during the lamp-treated process, leaving s-SWNT (blue, S) arrays.

In this work, we present a simple and reliable approach to prepare densely packed, well-aligned individual s-SWNT arrays using long-arc xenon-lamp (Xe-lamp) irradiation. First, we synthesized well-aligned individual SWNT arrays without curved or nonorientated tubes on a-plane sapphire using ethanol containing 3 wt % water as the carbon source. The mean density was ~20 tubes/μm. The m-SWNTs in the as-grown SWNT arrays on sapphire were preferentially destroyed by long-arc Xe-lamp irradiation, leaving s-SWNT arrays on the surface, as illustrated in Figure 1. Preferential destruction of the SWNTs with diameters smaller than 1 nm was also observed. Both resonant Raman spectra under 633 and 514 nm excitations and electrical characteristics revealed that Xe-lamp irradiation could effectively destroy m-SWNTs in the as-grown SWNT arrays. In general, for the SWNTs with diameters in the region of 1.15−1.55 nm, the percentage of s-SWNTs increases from ca. 50% to 95% after 60 min of irradiation. In situ $I-V$ measurement indicated that, with longer irradiation time, the on/off ratios of the FETs fabricated by the as-grown SWNT arrays increased from below 10 to well above 2000. This change clearly indicated that the m-SWNTs were destroyed faster than the s-SWNTs.

Experimental Section

A. Growth of SWNT Arrays. Single-polished a-plane (11−20) sapphire substrates (miscut angle <0.5°, surface roughness <5 Å) were bought from Hefei Kejing Materials Technology Co., China. After cleaning, the sapphire substrates were annealed at 1100 °C in air for 2 h, and thus, the interlaced atomic steps with ~0.5 nm height were observed by atomic force microscopy (AFM) (see Supporting Information Figure S1). Then $Fe(OH)_3$ colloids prepared by hydrolyzing $FeCl_3$ in boiling water were spin-coated on the substrate as catalysts. The SWNT growth was carried out in a low-pressure CVD system (Tystar Co.; the inner diameter of the quartz tube is 66 mm). After the substrate was heated to 850 °C in Ar, 2300 sccm of Ar and 300 sccm of H_2 were introduced for 5 min to reduce the catalysts. Then 45 sccm of Ar was bubbled through ethanol containing 3 wt % deionized (DI) water in a bubbler at a temperature of 30 °C for 5 min at atmospheric pressure to synthesize the SWNT arrays. As-grown SWNTs were characterized by scanning electron microscopy (SEM; Hitachi S4800 field emission, Japan), tapping-mode AFM (Veeco NanoScope IIIa, Veeco Co.), and Raman spectroscopy.

B. Long-Arc Xe-Lamp Irradiation. Figure 1 illustrates the schematic diagram of the irradiation experiment. SWNTs on sapphire or on SiO_2 substrates were exposed to a homemade 500 W long-arc Xe lamp, which has a continuous spectrum and was widely used as a solar simulator (see Supporting Information Figure S2). The intensity of the irradiation light at the substrate surface was maintained at ~75 mW/cm^2 (in the region of 0.18−11 μm wavelength, measured by a laser power/energy meter) by keeping the substrate surface perpendicular to the direction of the lamp light in air at room temperature, ~15 cm away from the Xe lamp in our case. Under this condition, the temperature near the substrate surface was below 50 °C after 60 min of continuous irradiation.

C. Raman Spectroscopy Characterization. Raman spectroscopy was used to probe the variation of the signals of m- and s-SWNTs. Resonant Raman spectra with 633 nm (1.96 eV) excitation (Renishaw micro-Raman system 1000, ~1 μm spot size, He−Ne laser) and 514 nm (2.41 eV) excitation (Renishaw micro-Raman system 2000, ~1 μm spot size, Ar^+ laser) were collected on 120 spots in the same area of one sample before and after each irradiation to compare the Raman signals. Normally, the interspot spacing was set as 50 μm parallel to the [1,−1,0,0] direction (growth direction of SWNTs) and 3 μm perpendicular to the [0,0,0,1] direction to avoid repeatedly collecting the Raman signal of the same SWNT.

D. Electrical Transport Property Characterization. Two kinds of samples, as-grown and irradiated SWNT arrays, were transferred from sapphire onto silicon with 1 μm or 300 nm SiO_2 by a polymer-mediated transfer method to fabricate FET devices.[41] Briefly, a polymer film was formed on the SWNT-containing substrate by spin-coating and soft baking. The film was then peeled off together with the nanotubes and was put on a target substrate. Finally, the polymer film was removed by washing away the polymer. The source and drain electrodes (normally Ti (3 nm)/Au (80 nm) or Ti (3 nm)/Pt (80 nm)) were predefined on the substrates by photolithography or electron beam lithography (EBL) before the SWNT arrays were transferred. The electrical transport properties were measured by a Keithley 4200-SCS semiconductor characterization system with a probe station in air at room temperature.

Results and Discussion

A. Growth of SWNT Arrays. Using ethanol containing 3 wt % water as the carbon source, we successfully synthesized well-aligned SWNT arrays with high coverage over a large scale on the a-plane sapphire substrates. Figure 2 shows the typical SEM and AFM images of the as-grown SWNT arrays. The low- and high-magnification SEM images (Figure 2a and the inset) indicate that the arrays are uniform over a large area. The growth direction of the SWNT arrays is perpendicular to the [0,0,0,1] direction of the a-plane sapphire, which was confirmed by SEM and Raman spectroscopy characterizations (see Supporting Information Figure S3), as consistent with the results reported

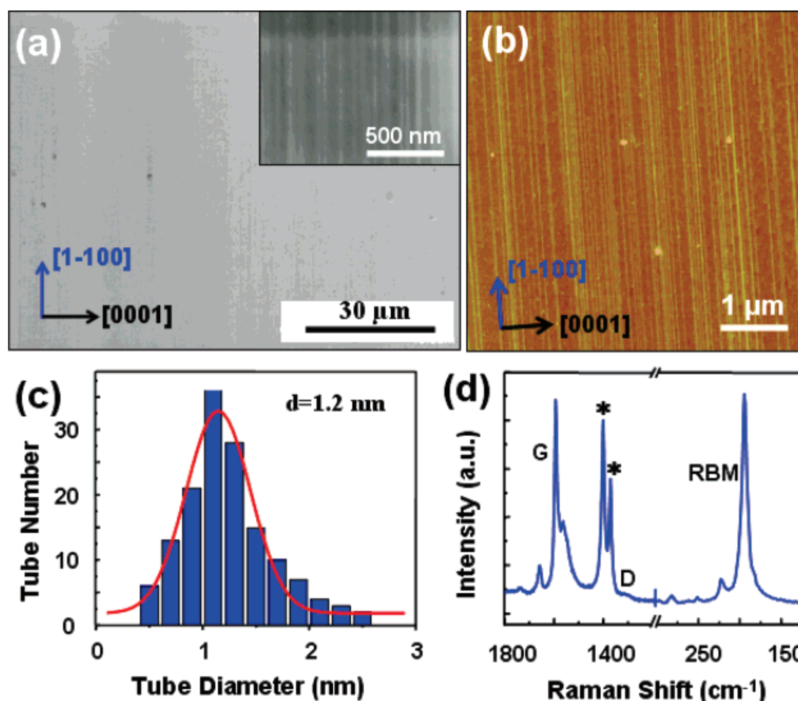

Figure 2. Characterizations of the well-aligned SWNT arrays grown on a-plane sapphire using ethanol containing 3 wt % water. (a, inset) Low- and high-magnification SEM images. (b) Typical AFM topographical image. (c) Histogram of the SWNT diameter distribution. The total number was 142, the line shows a Gaussian fitting curve, and the mean diameter is ~1.2 nm. (d) Typical Raman spectra with 633 nm excitation of the SWNT arrays. The peaks marked by asterisks at 1370 and 1400 cm^{-1} are from sapphire.

by Zhou et al.[29] Surprising precision of the alignment on annealed a-plane sapphire with interlaced atomic steps was further demonstrated by the following fact: We found a pair of SWNTs with a constant 14 nm intertube spacing for 5.72 μm instead of bundling together, implying that the misaligned angle was smaller than 0.14° and strongly suggesting the excellent alignment of the SWNT arrays (see Supporting Information Figure S4).

Curved or nonorientated tubes and amorphous carbon (a-C) were seldom observed (Figure 2b). No degradation of the alignment was found even when the tube density was higher than 20 tubes/μm. Interestingly, there even exists a 9 nm intertube spacing in the SWNT arrays, corresponding to a tube density of 111 tubes/μm (see Supporting Information Figure S5). This implies that the well-aligned individual SWNT arrays with much higher tube density (>100 tubes/μm) might be synthesized on a-plane sapphire under certain experimental conditions. The SWNTs could be tens of micrometers long. The mean diameter was 1.2 nm, and a few tubes with diameters larger than 2.5 nm were observed, implying that the arrays were composed of individual SWNTs, as shown in Figure 2c. Figure 2d shows typical Raman spectra of the SWNT arrays with 633 nm laser excitation (the two peaks at 1370 and 1400 cm^{-1} marked by asterisks are from sapphire). The peaks in the radical breathing mode (RBM) region further confirm that the as-grown tubes were SWNTs. In many cases, no D-band is observed around 1320 cm^{-1} (Figure 2d), indicating that the 3 wt % water does little damage to the nanotubes and the SWNTs are of high quality, although Joselevich et al.[30] observed a strong D-band and thus claimed that there existed a lot of defects on the SWNTs in their sample synthesized on sapphire.

It was found that the water in the ethanol played an important role in growing densely packed and well-aligned SWNT arrays on a-plane sapphire. Ethanol with 0, 2, 3, and 10 wt % water as the carbon source was used to grow SWNT arrays, and the corresponding results are shown in parts a–d, respectively, of Figure 3. With increasing water concentration, the sapphire surface becomes cleaner and cleaner, and it yields the best result when ethanol contains 3 wt % water. It is interesting that even when ethanol with 10 wt % water was used, SWNT arrays still could grow on the a-plane sapphire. However, the alignment became worse and the average nanotube length became shorter. Surprisingly, when the same experimental condition of >3 wt % water was used for silicon substrates, no carbon nanotube would grow, clearly showing that the sapphire plays an important role in the water-assisted growth of the aligned SWNT arrays as well. This suggests that the water in the ethanol had greatly suppressed the growth of SWNTs on the silicon surface due to the lack of enough carbon supply because sapphire has a much stronger ability to decompose hydrocarbon (ethanol) than silicon.

Figure 3e illustrates the role of water during the growth of the SWNT arrays. During the growth process, there are two kinds of ethanol molecules, ethanol(g) in the gas phase and ethanol(s) on the sapphire surface, which supply carbon atoms for the SWNT growth in the system. Because the ΔG of ethanol is negative at 850 °C, some ethanol molecules crack into a-C, and there exists a-C(g) in the gas phase and a-C(s) on the sapphire surface that contaminates the sapphire surface and poisons the catalyst particles, as shown by the red dotted arrows in Figure 3e. When a mild oxidizer, which in this case is the proper concentration of water molecules, is added to the system,[42] the a-C(g) and a-C(s) are selectively removed by the following reaction: $H_2O + C \rightarrow CO + H_2$, as shown by the blue dotted arrows in Figure 3e. As a result, the sapphire surface and the catalyst particles will be free of a-C contaminations. Therefore, on one hand, the guided forces originating from anisotropic interactions between the SWNT and the sapphire surface[29,30,35] can be kept well, which ensures the alignment of the SWNT arrays, even when the tube density is very high. On the other hand, the water gives a higher yield by removing a-C from the surfaces of the catalyst particles and keeping them

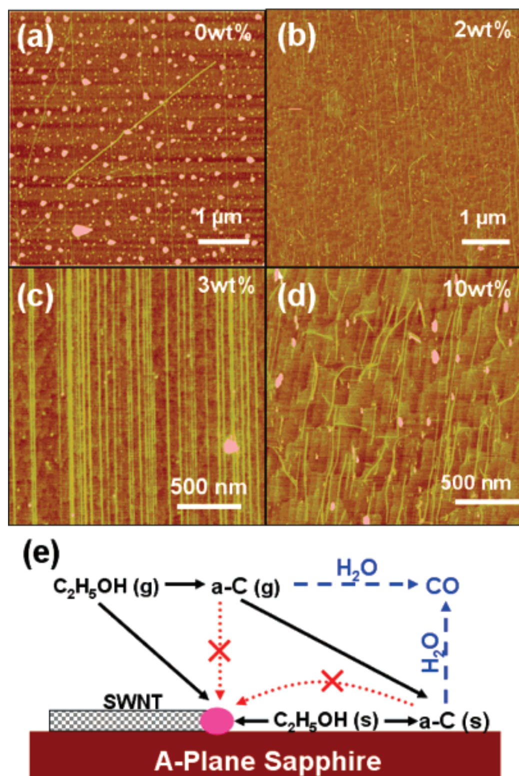

Figure 3. AFM images of the SWNTs grown on a-plane sapphire using ethanol containing different percentages of water and the schematic diagram of the role water plays during the growth process: (a) 0 wt %, (b) 2 wt %, (c) 3 wt %, (d) 10 wt %. (e) During the growth process, ethanol(g) in the gas phase and ethanol(s) adsorbed on the sapphire surface supply carbon atoms for the SWNT growth in the system. There is amorphous carbon (a-C) in the gas phase (a-C(g)) and on the sapphire (a-C(s)), contaminating the sapphire surface and poisoning the catalyst (red dotted arrows). The proper content of water vapor in the system keeps the sapphire surface clean by selectively removing a-C by the following reaction: $H_2O + C \rightarrow CO + H_2$ (blue dotted arrows).

alive longer. Accordingly, it eventually yields a high tube density without observable degradation of alignment.

B. Long-Arc Xe-Lamp Irradiation. Parts a and b of Figure 4 are low- and high-magnification AFM images of as-grown SWNT arrays on a-plane sapphire after Xe-lamp irradiation for 60 min. The higher magnification AFM image (Figure 4b) reveals that some SWNTs become discontinuous while others still appear to be continuous, indicating that the Xe-lamp irradiation process can indeed destroy some of the SWNTs. Further evidence is obtained by the AFM manipulation of the SWNTs. Figure 4c shows a typical AFM manipulation[43] result of the SWNT arrays on sapphire after 60 min of Xe-lamp irradiation. It is found that some of the SWNTs are dragged away while some are not. In contrast, in the as-grown SWNT arrays, all SWNTs can be stretched by the AFM manipulation. This indicates that those SWNTs which cannot be manipulated by the AFM are cut by the irradiation process.

Most interestingly, the AFM image clearly reveals the different responses of different diameter SWNTs to AFM manipulation. Most of the SWNTs with large diameters are stretched by the AFM tip. However, SWNTs with smaller diameters (d < 1 nm), as pointed out by the red arrows in the section analysis in Figure 4c, remain at the same place on the sapphire surface, with only a small incision at the place where the AFM tip passed. This indicates that the Xe-lamp irradiation can preferentially destroy SWNTs with small diameters, leaving discontinuous segments on the surface.

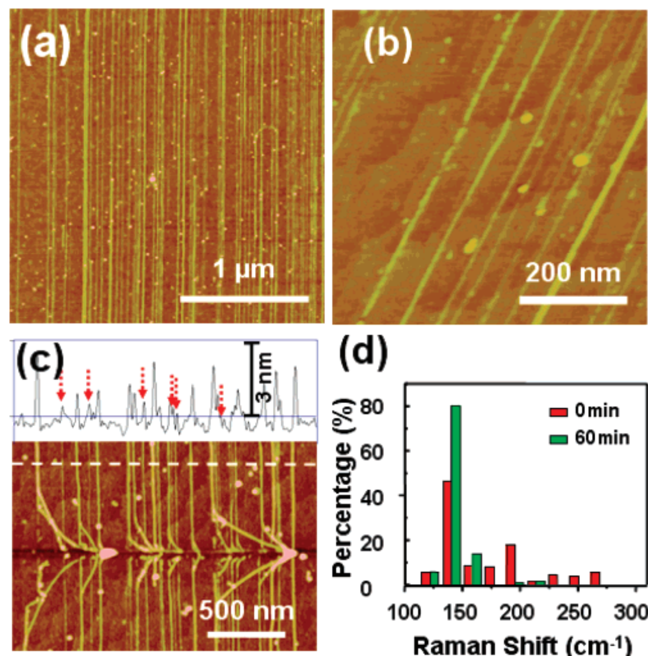

Figure 4. Characterizations of the light-treated SWNT arrays on a-plane sapphire. The arrays were exposed to a Xe lamp for 60 min at 75 mW/cm^2. (a) Low- and (b) high-magnification AFM images. (c) Typical AFM manipulation results. The section analysis is along the white dotted line in the image. The SWNTs with d < 1 nm cannot be stretched (red dotted arrows). (d) Histogram of the RBM signals with 633 nm excitation distribution before (red) and after (green) irradiation. The contents of the SWNTs with d < 1.3 nm (ω > 190 cm^{-1}) decrease after irradiation.

The selectivity on diameter of Xe-lamp irradiation was further confirmed by resonant Raman spectroscopy. Figure 4d is the histogram of the RBM distribution (under 633 nm excitation) of the SWNT arrays on a-plane sapphire before and after 60 min of Xe-lamp irradiation on the same sample. For SWNTs with small diameters (ω > 190 cm^{-1}, d < 1.3 nm; d is estimated using ω_{RBM} (cm^{-1}) = 248/[d (nm)][44]), their percentage dramatically decreases after irradiation; in contrast, the percentage of those with large diameters (ω < 190 cm^{-1}, d > 1.3 nm) increases a lot after irradiation. The results of the AFM manipulation and Raman spectroscopy both prove that the Xe-lamp irradiation can preferentially destroy SWNTs with small diameters (d < 1.3 nm).

C. Preferential Destruction of m-SWNTs Characterized by Resonant Raman Spectroscopy. Raman spectroscopy is a powerful tool to obtain the diameter, chirality, and electronic structure information of the SWNTs and is widely used to assign m/s types as well.[44] According to the correlation among the laser energy E, the RBM frequency ω, and the tube diameters d, the resonant Raman signals in certain RBM regions come from certain van Hove electronic transitions (E_{ii}) of m- or s-SWNTs.[16] For 633 nm excitation, RBM signals in the regions of 110−160, 160−220, and >240 cm^{-1} originate from the van Hove electronic transitions of s-SWNTs (E^{s}_{33}, E^{s}_{44}), m-SWNTs (E^{m}_{11}), and s-SWNTs (E^{s}_{22}), respectively. For 514 nm excitation, RBM signals (>130 cm^{-1}) in the regions of 130−150, 150−215, and 230−300 cm^{-1} originate from the van Hove electronic transitions of s-SWNTs (E^{s}_{44}), s-SWNTs (E^{s}_{33}), and m-SWNTs (E^{m}_{11}), respectively. As a result, m- and s-SWNTs in the region of 160−215 cm^{-1} (1.55 nm > d > 1.15 nm) can be detected with 633 and 514 nm excitations, respectively. Thus, the numbers and the relative content of m- and s-SWNTs in this

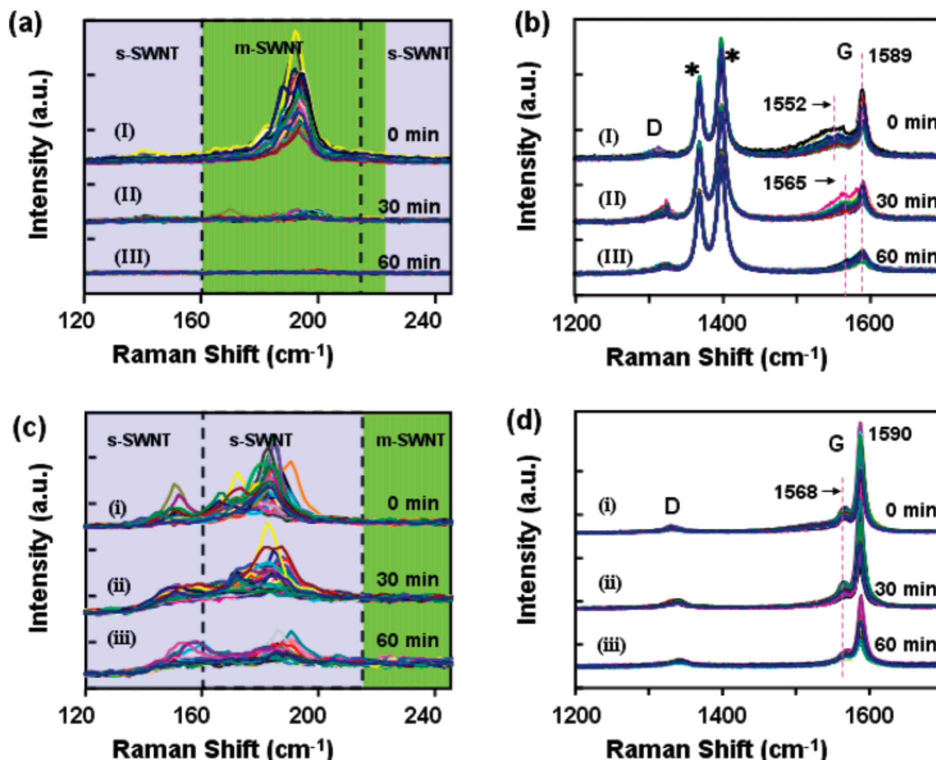

Figure 5. Normalized Raman spectra of the as-grown SWNT arrays on a-plane sapphire after 0 min (I, i), 30 min (II, ii), and 60 min (III, iii) of Xe-lamp irradiation. (a) RBM region and (b) D, G region with 633 nm excitation (normalized by the peak of sapphire at 1400 cm^{-1}). The peaks marked by asterisks in (b) at 1370 and 1400 cm^{-1} are from the sapphire substrate. (c) RBM region and (d) D, G region with 514 nm excitation (normalized by the peak of sapphire at 378 cm^{-1}). Each group of the spectra (I, II, III, i, ii, iii) contains the spectra collected from 39 spots in the same area of the same sample.

region can be evaluated from the resonant Raman spectra under 633 and 514 nm excitations by fitting the spectra with Lorentzian peaks.[45]

Figure 5 shows the normalized Raman spectra of the SWNT arrays on a-plane sapphire after 0 min (I, i), 30 min (II, ii), and 60 min (III, iii) of Xe-lamp irradiation with 633 nm (Figure 5a,b, normalized by the sapphire peak at 1400 cm^{-1}) and 514 nm (Figure 5c,d, normalized by the sapphire peak at 378 cm^{-1}) excitations. Each group of Raman spectra (I, II, III, i, ii, iii), composing 39 data spots, was collected from the same area but different spots on one sample. The two peaks at 1370 and 1400 cm^{-1} marked by asterisks in Figure 5b originate from the sapphire substrates.

As mentioned above, the Raman signals in the region of 160−215 cm^{-1} (1.55 nm > d > 1.15 nm) with 633 nm excitation (Figure 5a) originate from the first van Hove electronic transitions of m-SWNTs (E_{11}^{m}), representing the content of m-SWNTs, while the RBM signals with 514 nm excitation (Figure 5c) in the same region come from the third van Hove electronic transitions of s-SWNTs (E_{33}^{s}), representing the content of s-SWNTs. Comparing part a with part c of Figure 5, in the region of 160−215 cm^{-1}, there are many RBM signals originating from m-SWNTs (I-group) and s-SWNTs (i-group) in the as-grown SWNT arrays, implying that there exist both m-SWNTs and s-SWNTs before irradiation. After 30 min of Xe-lamp irradiation, the m-SWNT signals (II-group) dramatically weaken while the s-SWNT signals (ii-group) only decrease a little. When the irradiation time is increased to 60 min, almost no m-SWNT signals are left (III-group in Figure 5a) while a lot of s-SWNT signals (iii-group) remain. This shows that the Xe-lamp irradiation destroys the m-SWNTs much faster than the s-SWNTs, implying the preferential destruction of m-SWNTs compared with their semiconducting counterparts.

The preferential destruction of SWNTs with small diameters and m-SWNTs by Xe-lamp irradiation was further proved by the Raman spectra around the tangential mode (G and D) region with 633 nm (Figure 5b) and 514 nm (Figure 5d) excitations. The Breit−Wigner−Fano (BWF) peak around 1552 cm^{-1} (I-group in Figure 5b)[44,46] originates from the electron−phonon coupling in m-SWNTs, implying there are significant percentages of m-SWNTs in the as-grown SWNT arrays. After 60 min of irradiation (III-group), the BWF peak disappears, indicating that the m-SWNTs have been effectively destroyed. However, as for the tangential mode Raman signals of the s-SWNTs (∼1568 and ∼1590 cm^{-1}, Figure 5d), they remain almost unchanged after 30 min of irradiation (ii-group), compared with that of the as-grown SWNT arrays (i-group). Even after 60 min of irradiation, the Raman intensity only decreases a little (iii-group), which is consistent with the signals observed in the RBM region (Figure 5c), indicating the Xe-lamp irradiation has a much weaker effect on the s-SWNTs.

The preferential removal of SWNTs with small diameters by Xe-lamp irradiation can also be seen from Figure 5b,c. It can be seen from Figure 5c that, with increasing irradiation time (from the i-group to the ii- and iii-groups), the s-SWNTs with small diameters ($d \approx 1.3$ nm, around 190 cm^{-1}) are destroyed much faster than those with larger diameters ($d \approx 1.6$ nm, ∼150 cm^{-1}). The BWF peak frequency in Figure 5b shifts from ∼1552 cm^{-1} (I-group) to ∼1565 cm^{-1} (II-group) before it disappears (III-group), and the frequency separation Δ between the two components of the G-band feature decreases from ∼37 cm^{-1} (I-group, $\Delta \approx 1589$ cm^{-1} − 1552 cm^{-1} = 37 cm^{-1}) to ∼23 cm^{-1} (II-group, $\Delta \approx 1589$ cm^{-1} − 1565 cm^{-1} = 23 cm^{-1}) with increasing irradiation time, indicting that m-SWNTs with smaller diameters are preferentially destroyed because the BWF peak shifts to lower frequencies and the frequency separation

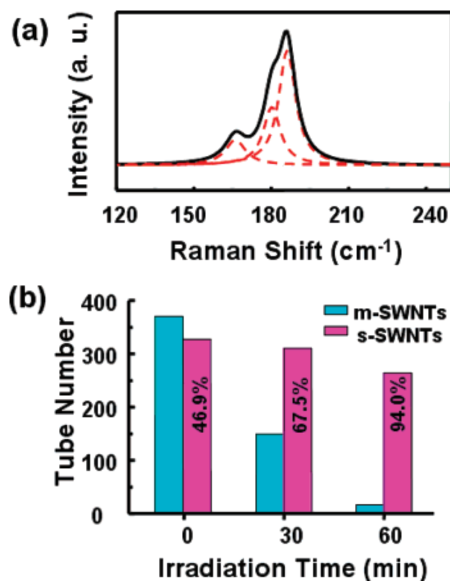

Figure 6. (a) Typical Raman spectral fitting by different Lorentzian peaks. The spectrum (under 633 nm excitation) is composed of three isolated Lorentzian peaks. (b) Percentage distributions of m- and s-SWNTs in the region of 160−215 cm^{-1} (1.15 nm < d < 1.55 nm) after 0, 30, and 60 min of irradiation. The numbers of m- and s-SWNTs were calculated from the spectral fitting results, under 633 and 514 nm excitations, respectively. The spectra under 633 and 514 nm excitations on 120 spots in the same area of the same sample were collected each time.

Δ becomes smaller as the diameter of the SWNTs gets smaller.[46] The width of the BWF peak decreases after 30 min of irradiation. This also indicates that the diameter distribution becomes narrower with increasing irradiation time.

To quantitatively study the relative destruction rate of m- and s-SWNTs during the Xe-lamp irradiation, the numbers of m- and s-SWNTs in the region of 1.15−1.55 nm (160−215 cm^{-1}) were estimated by the fitting of the corresponding resonant Raman spectra with thin Lorentzian peaks.[44,45,47] Figure 6a shows a typical fitting result, in which the Raman spectrum was composed of three isolated Lorentzian peaks, corresponding to three SWNTs. On the basis of the Raman spectra with 633 nm (1.96 eV) and 514 nm (2.41 eV) excitations after 0, 30, and 60 min of irradiation, the numbers of m- and s-SWNTs in the region of 1.15−1.55 nm after each irradiation time were calculated via reconstruction of the corresponding Raman spectra as shown in Figure 6b. Because, at each time, the Raman spectra were collected from the same SWNTs (some of them were destroyed with irradiation prolonged), we can evaluate the changes of the m- and s-SWNTs in the sample from the Raman spectra. It can be seen that the percentage of s-SWNTs rises from 46.9% (0 min) to 67.9% after 30 min of irradiation and eventually reaches 94.0% after 60 min of irradiation. A total of 59.7% (221 out of 370) of the m-SWNTs are destroyed after 30 min of irradiation, while only 5.2% (17 out of 327) of the s-SWNTs are destroyed. The calculated destruction rate of m-SWNTs is 13 times that of s-SWNTs in the first 30 min of irradiation. During the stage of 30−60 min, the number of the m-SWNTs decreases from 149 to 17 while that of the s-SWNTs changes from 310 to 264. Therefore, the destruction rate of m-SWNTs is only about 2.9 times that of s-SWNTs at this stage. This indicates that the majority of the m-SWNTs are removed at the early stages, and with increasing irradiation time, the destruction rate of m-SWNTs drops.

Therefore, as for the SWNTs with diameters in the region of 1.15−1.55 nm, the long-arc Xe-lamp irradiation can preferentially destroy m-SWNTs to obtain s-SWNT arrays. The percentage of s-SWNTs can be as high as 94% after 60 min of irradiation. The irradiation experiments of the nonorientated SWNTs synthesized on silicon dioxide using ethanol at 950 °C also show excellent preferential destruction of m-SWNTs (see Supporting Information Figure S6).

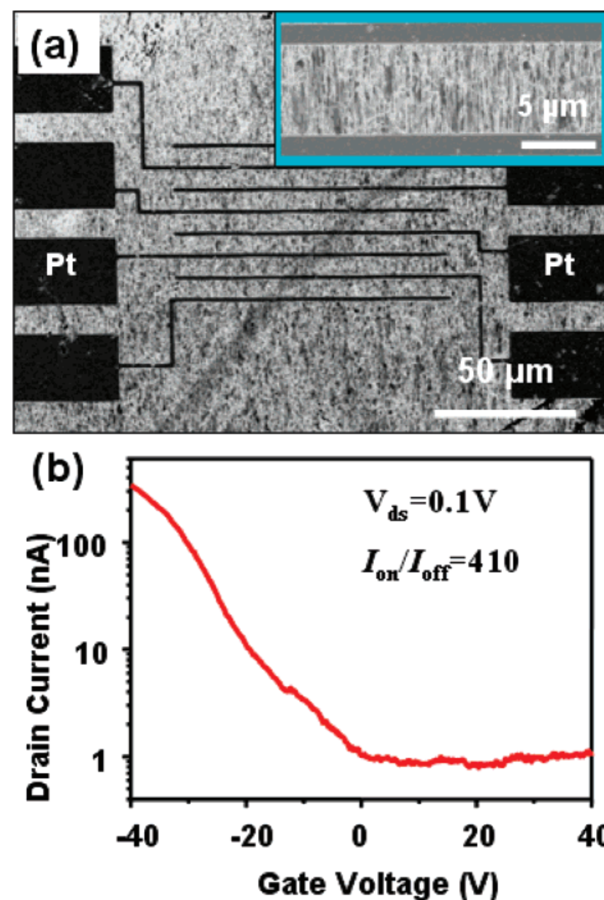

Figure 7. Transfer characteristics of the FET fabricated from SWNT arrays after 120 min of irradiation (s-SWNT arrays). The 120 min irradiated SWNT arrays on a-plane sapphire were transferred onto the silicon substrate with the EBL-predefined Pt electrodes atop 300 nm SiO_2 to form FETs. (a) SEM image of an FET device fabricated by an s-SWNT array. Inset: a pair of Pt electrodes connected by an s-SWNT array. (b) $I_{ds}-V_g$ curve of one FET of (a). The channel length was 6 μm, the width was 100 μm, and V_{ds} was 0.1 V.

D. Preferential Destruction of m-SWNTs Characterized by Electrical Characteristics. The preferential destruction of m-SWNTs was also characterized by electrical characteristics. Two kinds of samples, as-grown and irradiated SWNT arrays, were transferred onto silicon substrates with predefined electrodes to fabricate FET devices for electrical characteristics.

First, the as-grown SWNT arrays with 120 min of irradiation (the s-SWNTs were also characterized by Raman spectroscopy) were transferred onto silicon substrates, with EBL predefined Pt electrodes on 300 nm SiO_2, to fabricate FET devices. Figure 7a and the inset show the SEM images of representative FET devices. Figure 7b shows a typical $I_{ds}-V_g$ curve of an FET constructed by the s-SWNT arrays (channel length $L = 6$ μm, width $W = 100$ μm). V_{ds} was 0.1 V. The FET can be switched off at positive gate voltages (V_g). The on/off ratio is about 420, which is much larger than that (∼170) achieved by the electrical breakdown results of the same electrode size (see Supporting Information Figure S7).

The above results imply that the FET should be constructed with s-SWNTs since the FET will be electrically shorted by

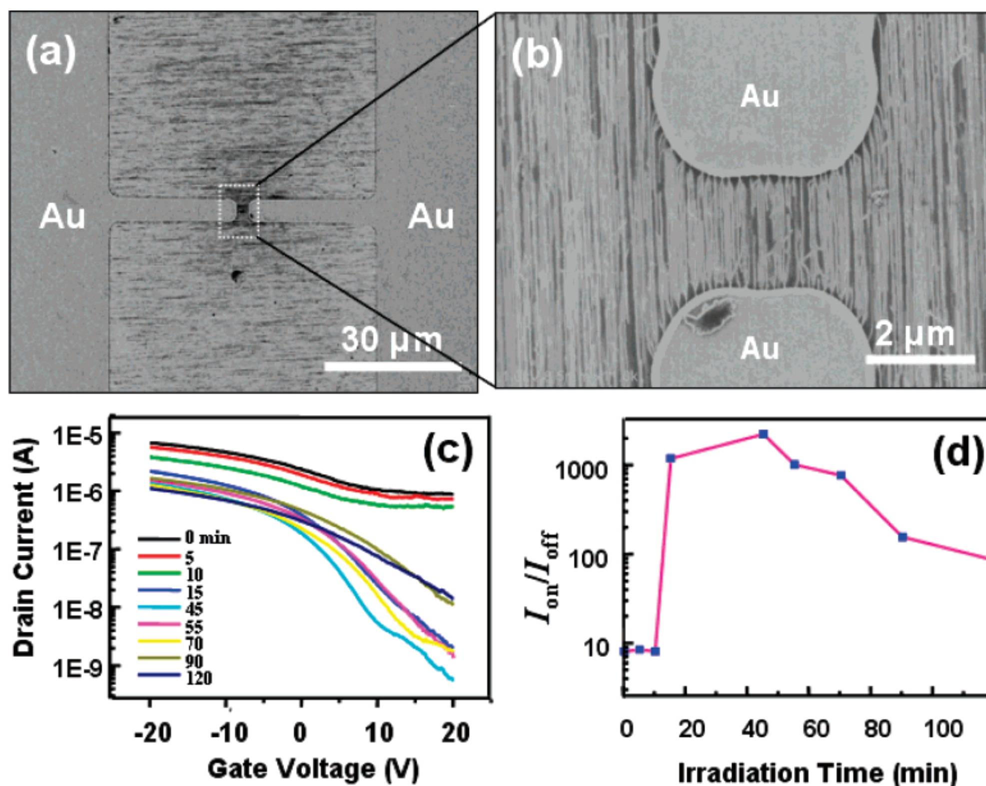

Figure 8. Transfer characteristics of the FET fabricated from SWNT arrays with longer irradiation times. The nonirradiated SWNT arrays on a-plane sapphire were transferred onto the photolithographically predefined Au electrodes on 1 μm SiO_2 to form FET devices. The channel length was ~3 μm. (a, b) SEM images of an FET device fabricated by nonirradiated SWNT arrays. (c) $I_{ds}-V_g$ plots after different Xe-lamp irradiation times (0, 5, 10, 15, 45, 75, 90, and 120 min) of one FET of (a). V_{ds} was 0.1 V. (d) I_{on}/I_{off} vs irradiation time of (c).

the m-SWNTs connecting the source and drain, eventually resulting in a low on/off ratio. The on-state current of the FETs is very low, only about 350 nA under 0.1 V. This might result from the following: (1) The 120 min irradiation not only destroyed all the m-SWNTs, but also caused some damage to the s-SWNTs in the arrays, so the lengths of the s-SWNTs might be too short to span the source/drain electrodes. (2) The contact between the as-transferred s-SWNTs and the Pt electrodes was poor. However, the $I_{ds}-V_g$ curve of the FET proves that the Xe-lamp irradiation can effectively remove m-SWNTs with different diameters; thus, s-SWNT arrays and s-SWNT FETs were fabricated.

To solve the above problems, the second kind of SWNT arrays, i.e., as-grown SWNT arrays, were transferred onto silicon substrates, with photolithographically predefined Au electrodes on 1 μm SiO_2, to fabricate FET devices and perform the electrical characteristics. In this case, the performance of the FETs can be measured by in situ increasing the light-treatment time. Parts a and b of Figure 8 show typical SEM images of the device. There are about 100−300 SWNTs spanning the ~3 μm channel. The SWNTs formed small bundles at the edge of the metal electrodes. The V_{ds} was 0.1 V. Figure 8c shows the $I_{ds}-V_g$ plots of the FET device with Xe-lamp irradiation times of 0, 5, 10, 15, 45, 55, 70, 90, and 120 min. The device exhibits a p-type FET behavior in air at room temperature. After 10 min of irradiation, the on-state and off-state currents decrease slowly and the FET cannot be turned off, implying that part of the SWNTs are destroyed and there still exist some m-SWNTs. After 15 min of irradiation, the off-state current dramatically decreases to below 1 nA together with a slight decrease of the on-state current, and the device is turned off completely. This means that all m-SWNTs have been destroyed, leaving only s-SWNTs that spanned the source/drain electrodes. From the results of Figures 5 and 6, the RBM signals of m-SWNTs decrease more than 10 times faster than those of s-SWNTs at the early stage of irradiation, so the m-SWNTs in the device could be quickly destroyed since there were only 100−300 SWNTs in each FET device.

Figure 8d shows the on/off ratios corresponding to the curves in Figure 8c. With increasing irradiation time, the semiconducting property of the SWNT arrays remains unchanged in a large time span. After 10 min of irradiation, the on/off ratio is only 7.4, without an observable change compared with that of the nonirradiated result. The on/off ratio rises sharply to 1086 after 15 min of irradiation and reaches 2044 after 45 min of irradiation. After that, the off-state current begins to increase slowly, together with the on-state current. We speculate that the improvement of the contact during the irradiation process and/or the formation of a-C originating from the decomposition of SWNTs and/or from the residual polymer during the irradiation process might have led to the increase of the on- and off-state currents when the irradiation time was longer than 45 min. We show that Xe-lamp irradiation can preferentially remove m-SWNTs in the transferred SWNT arrays on silicon substrates, thus greatly improving the performance of FET devices. It also supplies a parallel and simple route for the large-scale preparation of s-SWNT-based devices.

Conclusion

We report in this paper a simple and reliable approach to prepare densely packed, well-aligned individual s-SWNT arrays using long-arc Xe-lamp irradiation. The densely packed well-aligned individual SWNT arrays were first synthesized parallel to the [1,−1,0,0] direction on a-plane sapphire from ethanol containing 3 wt % water. The density is ~20 tubes/μm without degradation of the alignment. The water in ethanol plays a key role in the improvement of the density and orientation of the

arrays by keeping the sapphire surface and the catalysts free of the a-C contaminants. The s-SWNT arrays were then fabricated by long-arc Xe-lamp irradiation. It is found that the Xe-lamp irradiation can preferentially destroy the SWNTs with small diameters ($d < 1$ nm) and the m-SWNTs in the arrays, as proved by AFM, Raman spectroscopy, and electrical transport measurement characterizations. Raman spectroscopy with 633 and 514 nm excitations was used to probe the change of the m- and s-SWNT content in the region of 160−215 cm^{-1} after different periods of irradiation, and it shows that the m-SWNTs are destroyed at a rate ∼13 times that of s-SWNTs in the first 30 min and the percentage of s-SWNTs increases from ∼50% to ∼95% after 60 min of irradiation. Furthermore, two kinds of SWNTs samples, as-grown SWNT arrays and SWNT arrays after 120 min of irradiation, were transferred onto silicon substrates with metal electrodes and were constructed into FETs; thus, the electrical transport properties of the s-SWNT arrays clearly indicate that the m-SWNTs are destroyed faster than the s-SWNTs. The as-prepared s-SWNT arrays are of great importance in fabricating s-SWNT devices. The Xe-lamp irradiation approach can be easily combined with modern photolithographic techniques and find its position in the integration of s-SWNT devices in large scale.

Acknowledgment. This work was supported by NSFC (Grants 20573002, 20673004, 20725307, and 50521201) and MOST (Grants 2006CB932701, 2006CB932403, and 2007CB936203).

Supporting Information Available: AFM characterization of the annealed a-plane sapphire substrate, spectrum of the long-arc Xe lamp, polarized Raman spectral characterizations of the growth direction of the SWNT arrays, AFM characterizations of the 14 nm intertube spacing, AFM characterizations of the 9 nm intertube spacing, SEM and Raman characterizations of the irradiation results of the SWNT films grown on SiO_2, and electrical breakdown results of the as-grown SWNT arrays. This material is available free of charge via the Internet at http://pubs.acs.org.

References and Notes

(1) Durkop, T.; Getty, S. A.; Cobas, E.; Fuhrer, M. S. *Nano Lett.* **2004**, *4* (1), 35−39.

(2) Zhou, X. J.; Park, J. Y.; Huang, S. M.; Liu, J.; McEuen, P. L. *Phys. Rev. Lett.* **2005**, *95* (14), 146805.

(3) Yao, Z.; Kane, C. L.; Dekker, C. *Phys. Rev. Lett.* **2000**, *84* (13), 2941−2944.

(4) Lin, Y. M.; Appenzeller, J.; Knoch, J.; Avouris, P. *IEEE Trans. Nanotechnol.* **2005**, *4* (5), 481−489.

(5) Bachtold, A.; Hadley, P.; Nakanishi, T.; Dekker, C. *Science* **2001**, *294* (5545), 1317−1320.

(6) Chen, Z. H.; Appenzeller, J.; Lin, Y. M.; Sippel-Oakley, J.; Rinzler, A. G.; Tang, J. Y.; Wind, S. J.; Solomon, P. M.; Avouris, P. *Science* **2006**, *311* (5768), 1735−1735.

(7) Kang, S. J.; Kocabas, C.; Ozel, T.; Shim, M.; Pimparkar, N.; Alam, M. A.; Rotkin, S. V.; Rogers, J. A. *Nat. Nanotechnol.* **2007**, *2* (4), 230−236.

(8) Chen, J.; Perebeinos, V.; Freitag, M.; Tsang, J.; Fu, Q.; Liu, J.; Avouris, P. *Science* **2005**, *310* (5751), 1171−1174.

(9) Misewich, J. A.; Martel, R.; Avouris, P.; Tsang, J. C.; Heinze, S.; Tersoff, J. *Science* **2003**, *300* (5620), 783−786.

(10) Kong, J.; Franklin, N. R.; Zhou, C. W.; Chapline, M. G.; Peng, S.; Cho, K. J.; Dai, H. J. *Science* **2000**, *287* (5453), 622−625.

(11) Allen, B. L.; Kichambare, P. D.; Star, A. *Adv. Mater.* **2007**, *19* (11), 1439−1451.

(12) Zheng, M.; Jagota, A.; Strano, M. S.; Santos, A. P.; Barone, P.; Chou, S. G.; Diner, B. A.; Dresselhaus, M. S.; McLean, R. S.; Onoa, G. B.; Samsonidze, G. G.; Semke, E. D.; Usrey, M.; Walls, D. J. *Science* **2003**, *302* (5650), 1545−1548.

(13) Zheng, M.; Jagota, A.; Semke, E. D.; Diner, B. A.; Mclean, R. S.; Lustig, S. R.; Richardson, R. E.; Tassi, N. G. *Nat. Mater.* **2003**, *2* (5), 338−342.

(14) Zheng, M.; Semke, E. D. *J. Am. Chem. Soc.* **2007**, *129* (19), 6084−6085.

(15) Arnold, M. S.; Green, A. A.; Hulvat, J. F.; Stupp, S. I.; Hersam, M. C. *Nat. Nanotechnol.* **2006**, *1* (1), 60−65.

(16) Strano, M. S.; Dyke, C. A.; Usrey, M. L.; Barone, P. W.; Allen, M. J.; Shan, H. W.; Kittrell, C.; Hauge, R. H.; Tour, J. M.; Smalley, R. E. *Science* **2003**, *301* (5639), 1519−1522.

(17) Toyoda, S.; Yamaguchi, Y.; Hiwatashi, M.; Tomonari, Y.; Murakami, H.; Nakashima, N. *Chem.*−*Asian J.* **2007**, *2* (1), 145−149.

(18) An, L.; Fu, Q. A.; Lu, C. G.; Liu, J. *J. Am. Chem. Soc.* **2004**, *126* (34), 10520−10521.

(19) Collins, P. C.; Arnold, M. S.; Avouris, P. *Science* **2001**, *292* (5517), 706−709.

(20) Bachilo, S. M.; Balzano, L.; Herrera, J. E.; Pompeo, F.; Resasco, D. E.; Weisman, R. B. *J. Am. Chem. Soc.* **2003**, *125* (37), 11186−11187.

(21) Li, Y. M.; Mann, D.; Rolandi, M.; Kim, W.; Ural, A.; Hung, S.; Javey, A.; Cao, J.; Wang, D. W.; Yenilmez, E.; Wang, Q.; Gibbons, J. F.; Nishi, Y.; Dai, H. J. *Nano Lett.* **2004**, *4* (2), 317−321.

(22) Zhang, G. Y.; Qi, P. F.; Wang, X. R.; Lu, Y. R.; Li, X. L.; Tu, R.; Bangsaruntip, S.; Mann, D.; Zhang, L.; Dai, H. J. *Science* **2006**, *314* (5801), 974−977.

(23) Huang, H. J.; Maruyama, R.; Noda, K.; Kajiura, H.; Kadono, K. *J. Phys. Chem. B* **2006**, *110* (14), 7316−7320.

(24) Seidel, R.; Graham, A. P.; Unger, E.; Duesberg, G. S.; Liebau, M.; Steinhoegl, W.; Kreupl, F.; Hoenlein, W. *Nano Lett.* **2004**, *4* (5), 831−834.

(25) Huang, S. M.; Cai, X. Y.; Liu, J. *J. Am. Chem. Soc.* **2003**, *125* (19), 5636−5637.

(26) Hong, B. H.; Lee, J. Y.; Beetz, T.; Zhu, Y. M.; Kim, P.; Kim, K. S. *J. Am. Chem. Soc.* **2005**, *127* (44), 15336−15337.

(27) Zhang, Y. G.; Chang, A. L.; Cao, J.; Wang, Q.; Kim, W.; Li, Y. M.; Morris, N.; Yenilmez, E.; Kong, J.; Dai, H. *J. Appl. Phys. Lett.* **2001**, *79* (19), 3155−3157.

(28) Joselevich, E.; Lieber, C. M. *Nano Lett.* **2002**, *2* (10), 1137−1141.

(29) Han, S.; Liu, X. L.; Zhou, C. W. *J. Am. Chem. Soc.* **2005**, *127* (15), 5294−5295.

(30) Ismach, A.; Segev, L.; Wachtel, E.; Joselevich, E. *Angew. Chem., Int. Ed.* **2004**, *43* (45), 6140−6143.

(31) Kocabas, C.; Hur, S. H.; Gaur, A.; Meitl, M. A.; Shim, M.; Rogers, J. A. *Small* **2005**, *1* (11), 1110−1116.

(32) Kocabas, C.; Shim, M.; Rogers, J. A. *J. Am. Chem. Soc.* **2006**, *128* (14), 4540−4541.

(33) Ago, H.; Nakamura, K.; Ikeda, K.; Uehara, N.; Ishigami, N.; Tsuji, M. *Chem. Phys. Lett.* **2005**, *408* (4−6), 433−438.

(34) Ismach, A.; Kantorovich, D.; Joselevich, E. *J. Am. Chem. Soc.* **2005**, *127* (33), 11554−11555.

(35) Ago, H.; Uehara, N.; Ikeda, K.; Ohdo, R.; Nakamura, K.; Tsuji, M. *Chem. Phys. Lett.* **2006**, *421* (4−6), 399−403.

(36) Kocabas, C.; Meitl, M. A.; Gaur, A.; Shim, M.; Rogers, J. A. *Nano Lett.* **2004**, *4* (12), 2421−2426.

(37) Rao, S. G.; Huang, L.; Setyawan, W.; Hong, S. H. *Nature* **2003**, *425* (6953), 36−37.

(38) Wang, Y. H.; Maspoch, D.; Zou, S. L.; Schatz, G. C.; Smalley, R. E.; Mirkin, C. A. P. *Natl. Acad. Sci. U.S.A.* **2006**, *103* (7), 2026−2031.

(39) Yan, Y. H.; Chan-Park, M. B.; Zhang, Q. *Small* **2007**, *3* (1), 24−42.

(40) Li, X. L.; Zhang, L.; Wang, X. R.; Shimoyama, I.; Sun, X. M.; Seo, W. S.; Dai, H. J. *J. Am. Chem. Soc.* **2007**, *129* (16), 4890−4891.

(41) Jiao, L. Y.; Liu, Z. F. Unpublished data.

(42) Hata, K.; Futaba, D. N.; Mizuno, K.; Namai, T.; Yumura, M.; Iijima, S. *Science* **2004**, *306* (5700), 1362−1364.

(43) Duan, X. J.; Zhang, J.; Ling, X.; Liu, Z. F. *J. Am. Chem. Soc.* **2005**, *127* (23), 8268−8269.

(44) Dresselhaus, M. S.; Dresselhaus, G.; Jorio, A.; Souza, A. G.; Saito, R. *Carbon* **2002**, *40* (12), 2043−2061.

(45) Luo, Z. T.; Pfefferle, L. D.; Haller, G. L.; Papadimitrakopoulos, F. *J. Am. Chem. Soc.* **2006**, *128* (48), 15511−15516.

(46) Brown, S. D. M.; Jorio, A.; Corio, P.; Dresselhaus, M. S.; Dresselhaus, G.; Saito, R.; Kneipp, K. *Phys. Rev. B* **2001**, *6315* (15), 81401.

(47) Strano, M. S. *J. Am. Chem. Soc.* **2003**, *125* (51), 16148−16153.